Search for pressure-induced quantum criticality in YbFe_{2}Zn_{20}

S. K. Kim, M. S. Torikachvili, S. L. Bud'ko, and P. C. Canfield

Phys. Rev. B **88**, 045116 — Published 12 July 2013

DOI: 10.1103/PhysRevB.88.045116

Search for Pressure Induced Quantum Criticality in $YbFe_2Zn_{20}$

S. K. Kim,[1,2] M. S. Torikachvili,[2,3] S. L. Bud'ko,[1,2] and P. C. Canfield[1,2]

[1]*Ames Laboratory, Iowa State University, Ames, Iowa 50011, USA*
[2]*Department of Physics and Astronomy, Iowa State University, Ames, Iowa 50011, USA*
[3]*Department of Physics, San Diego State University, San Diego, California 92182, USA*

Electrical transport measurements of the heavy fermion compound $YbFe_2Zn_{20}$ were carried out under pressures up to 8.23 GPa and down to temperatures of nearly 0.3 K. The pressure dependence of the low temperature Fermi-liquid state was assessed by fitting $\rho(T) = \rho_0 + AT^n$ with $n = 2$ for $T < T_{\rm FL}$. Power law analysis of the low temperature resistivities indicates $n = 2$ over a broad temperature range for $P \lesssim 5$ GPa. However, at higher pressures, the quadratic temperature dependence is only seen at the very lowest temperatures, and instead shows a wider range of $n < 2$ power law behavior in the low temperature resistivities. As pressure was increased, $T_{\rm FL}$ diminished from ~ 11 K at ambient pressure to ~ 0.6 K at 8.23 GPa. Over the same pressure range, the A parameter increased dramatically with a functional form of $A \propto (P - P_{\rm c})^{-2}$ with $P_{\rm c} \simeq 9.8$ GPa being the critical pressure for a possible quantum critical point.

PACS numbers: 62.50.-p,72.15.Eb,72.15.Qm,75.20.Hr,75.30.Kz

I. INTRODUCTION

Strongly correlated electron systems manifest a rich variety of electronic and magnetic properties that have fascinated scientists for decades; Mott insulators,[1] exotic superconductors,[2,3] and heavy fermions[4–6] continue to be topics of intense study. Heavy fermions are a subset of materials known as Kondo lattices. In a Kondo lattice system, near the characteristic Kondo temperature, $T_{\rm K}$, the moment bearing ions in the lattice each act as a Kondo impurity, with which the conduction electrons hybridize and create a screening cloud of dynamically polarized electrons. At lower temperatures, the conduction electrons become coherent and manifest Fermi-liquid (FL) behavior. This leads to a myriad of novel features in measurements of the Kondo lattice's thermodynamic and transport properties at and below $T_{\rm K}$: the susceptibility, which has a local moment-like, paramagnetic behavior at high temperatures, shows a loss of local moment behavior below $T_{\rm K}$; in measurements of specific heat, a large Sommerfeld coefficient for $T < T_{\rm K}$ points to a large effective electron mass; resistivity measurements for $T \ll T_{\rm K}$ are Fermi-liquid-like and are consistent with a large electronic density of states at the Fermi energy.

The $YbTM_2Zn_{20}$ (TM = Fe, Co, Ru, Rh, Os, and Ir) compounds form a family of Yb-based heavy fermions where subtle changes in the hybridization of the Yb local moment with the conduction electrons can be achieved by changing the transition metal (TM) element. These materials show classical heavy fermion behavior in their physical properties.[7–11] Of this series, $YbCo_2Zn_{20}$ seems to be an outlier with T_K much lower than those of the other five members ($T_{\rm K}$ = 33, 30, 16, 20, and 21 K for TM = Fe, Ru, Rh, Os, and Ir, respectively, and $T_{\rm K}$ = 1.5 K for TM = Co).[7] Specific heat measurements yielded large Sommerfeld constants (γ = 520, 580, 740, 580, 540 mJ/mol K^2 for TM = Fe, Ru, Rh, Os, and Ir, respectively, and an exceptionally large value of 7200 mJ/mol K^2 for $YbCo_2Zn_{20}$).[7,10] Magnetic susceptibility measurements show Curie-Weiss behavior at high temperatures and a broad maximum at low temperatures, signalling a Kondo screened local moment. When the magnetic component of the resistivity is isolated by subtracting from it the resistivity of the non-magnetic counterpart $LuTM_2Zn_{20}$, the resistivities of all members of the $YbTM_2Zn_{20}$ series show a local maximum near $T_{\rm K}$. Below $T_{\rm K}$, the coherent scattering of electrons decreases the resistivity until at very low temperatures, a wide temperature range of T^2 behavior signals the onset of Fermi-liquid behavior.[12]

Although no indication of low temperature, local moment order was found for any of the $YbTM_2Zn_{20}$ compounds,[7–11] by combining the idea of the basic Doniach model[13] with simple steric arguments, it is anticipated that the application of pressure will stabilize local-moment-like states in Yb-based Kondo lattic systems. Indeed under pressure, indications of a magnetic instability were seen in $YbCo_2Zn_{20}$. When a modest pressure of ~ 1 GPa was applied, the resistivity measurement showed an anomaly, possibly magnetic in origin, at ~ 0.15 K.[14,15] A more recent study claims that a quantum critical point exists near 1.8 GPa with magnetic order existing on the high pressure side.[16]

Based on our earlier work on the RTM_2Zn_{20} compounds, and specifically the $YbTM_2Zn_{20}$ heavy fermions,[7–11,17–19] we chose $YbFe_2Zn_{20}$ for a systematic study of the pressure and temperature dependent electrical resistivity for 300 mK $< T <$ 300 K and $P <$ 8.3 GPa. The RFe_2Zn_{20} and RCo_2Zn_{20} series manifest clear de Gennes scaling of their characteristic ordering temperatures with the RFe_2Zn_{20} compounds having over an order of magnitude higher ordering temperatures. Using this as a caliper of the upper limit of potential Yb-local moment ordering, $YbFe_2Zn_{20}$ may manifest pressure induced magnetic ordering as high as 1 K. In addition the RFe_2Zn_{20} compounds (R = Gd - Tm) all manifest ferromagnetic order rather than the antiferromagnetic order manifested by the RCo_2Zn_{20} materials. $YbFe_2Zn_{20}$

then also offers the possibility of evolving from a heavy fermion ground state to an ordered state with ferromagnetic character. $YbFe_2Zn_{20}$ also shows the clearest evidence of having the whole $J = 7/2$ Hunds rule ground-state degeneracy (i.e. the whole $R\ln 8$ entropy) being involved in the Kondo state. As such, this system offers a clear contrast to many QCP systems in which the entropy under discussion is the $R\ln 2$ associated with the lowest lying Kramers doublet. Given the fact that the Kondo temperature of $YbFe_2Zn_{20}$ is roughly an order of magnitude larger than that for $YbCo_2Zn_{20}$ we anticipate that the pressure needed to bring $YbFe_2Zn_{20}$ to a potential quantum critical point (or at least quantum phase transition) will be on the order of 10 GPa. In this work we show that, based on measurements of the temperature dependent electrical resistivity under pressures up to 8.23 GPa and the observed divergence of the coefficient of its T^2 component as $1/(P-P_c)^2$, $YbFe_2Zn_{20}$ very likely has a quantum critical point located near $P_c = 9.8$ GPa.

II. EXPERIMENTAL METHODS

The single crystals used for this paper were taken from the batches made for previous studies of $YbFe_2Zn_{20}$.[7,11] The crystals were grown using the techniques described extensively in the pioneering work on the RTM_2Zn_{20} materials presented in Ref. 9,10,17–19. Briefly, elemental Yb, Fe, and Zn were placed in an alumina crucible in the molar ratio 2:4:94. A second, "catch," crucible filled with silica wool and the growth crucible were sealed in a silica tube that was back filled with roughly a quarter atmosphere of high purity argon.[20,21] The sealed ampoule was then placed in a high temperature furnace, heated over 5 hours to between 900 °C and 1000 °C and then cooled slowly (over 65-85 hours) to 600 °C, at which point the excess, Zn rich solution was decanted from the large, well faceted single crystals of $YbFe_2Zn_{20}$. A similar process was used for the growth of the $LuFe_2Zn_{20}$ crystal.

For resistivity measurements, the single crystals were polished down to appropriate dimensions for the two types of pressure cells used: typically $1.6 \times 0.5 \times 0.4$ mm^3 for the piston cylinder cell ($P \lesssim 2$ GPa)[22,23] and typically $700 \times 150 \times 30$ μm^3 for the modified Bridgman anvil cells (mBAC) ($2.85 \leq P \leq 8.23$ GPa).[24] The small sizes of the samples used in these pressure cells led to relatively large geometric errors in the resistivity values. Therefore, all resistivity measurements were normalized to that of a single measurement on a large sample which was used in a previous study on the transport properties of Yb-based heavy fermions.[9,10] This normalization was done by multiplicatively matching the resistivity of a given sample at ambient pressure and 298 K to that from Refs. 9,10. Then the same multiplicative value was applied to all subsequent resistivity measurements done at progressively higher pressures with that pressure cell. This method of normalization was done for all four sets of resistivity measurements.

Given that these materials have cubic unit cells,[7–10,17] this normalization procedure is considered to be quite reliable. Under pressure, it is also expected that the cubic symmetry is minimally affected by the non-isotropic nature of reduced hydrostaticity.

At ambient pressure, $YbFe_2Zn_{20}$ samples had residual resistivity ratios (RRR) that varied from 18 to 38. The RFe_2Zn_{20} compounds can have a small width of formation with regard to Fe. This was examined in detail for the case of $TbFe_2Zn_{20}$ in Ref. 9. The $YbFe_2Zn_{20}$ and $LuFe_2Zn_{20}$ samples manifest relatively low disorder scattering,with RRR values of 18 and 13, respectively. The small variation in RRR between individual $YbFe_2Zn_{20}$ crystals as well as between $YbFe_2Zn_{20}$ and $LuFe_2Zn_{20}$ crystals which may be associated with small differences in purity/composition.

The piston cylinder cell was used for pressure measurements up to about 2 GPa.[22,23] This cell was designed to be used in a Quantum Design Physical Properties Measurement System (PPMS) with the dc resistivity option. The cell was fitted with a NiCrAl inner core and the pressure medium was a mixture of 6 : 4 n-pentane : mineral oil. At room temperature, the pressure inside the cell was monitored by using the resistance of a Manganin wire and at low temperatures, the superconducting transition temperature of a lead sample was used.[25]

A modified Bridgman anvil cell was used for resistivity measurements at pressures up to about 8.3 GPa. This cell has been designed to work inside a PPMS and has been modified to use a liquid pressure medium.[24] For this study, two pressure media were used with the mBAC: a mixture of 1 : 1 n-pentane : iso-pentane and a mixture of 1 : 1 Fluorinert 70 : Fluorinert 770 (1 : 1 FC70 : FC770).[26–29] Despite the the lower pressure of solidification at room temperature of the latter liquid medium, its lower compressibility allowed higher pressures to be more readily achieved. As in the piston cylinder cell, the superconducting (SC) transition temperature of a lead sample was used as a pressure gauge within the mBAC sample space. The width of the SC transition of the lead manometer can be used as an estimate of the pressure gradients within the sample space. For the mBAC, at the highest pressure using the 1 : 1 FC70 : FC770 mixture (8.23 GPa), the width of the SC transition suggests a relatively small pressure gradient of 0.24 GPa exists across the lead sample. At the lowest pressure with the 1 : 1 FC70 : FC770 mixture (3.62 GPa), the pressure gradient was closer to 0.15 GPa.

The low-temperature resistivity follows $\rho(T) = \rho_0 + AT^2$ with the average ambient pressure value of A $7.0 \pm 0.3 \times 10^{-10}$ Ω cm K^2. It should be noted that with two different pressure cells and three different liquid media, there are clear, albeit small, differences between the various pressure dependent data sets, that may (in part) be attributed to cell to cell and/or sample to sample differences but these are small compared to the much larger changes due to pressure (see Fig. 8 below and associated discussion).

For low temperature measurements, down to nearly 0.3 K, a CRYO Industries of America ^{3}He system was used to measure samples under pressure with the mBAC.

For most pressure cells, one cycle of cooling and warming causes a pressure cell to thermally contract and expand. One subtlety of pressure measurements with the mBAC is that this thermal cycling can induce a modest pressure increase within the pressure cell. This is the origin of the slight pressure differences between subsequent measurements with the PPMS (used for measurements down to 2 K) and the ^{3}He system (used for measurements down to nearly 0.3 K). An example of this effect is seen below in Fig. 3.

III. RESULTS

Temperature dependent resistivity measurements of $YbFe_2Zn_{20}$, at ambient pressure and under pressures up to 2.03 GPa, are shown in Fig. 1. These measurements were taken using a piston cylinder cell. At ambient pressure, as temperature is decreased from 300 K (inset of Fig. 1) the resistivity decreases in a near-linear manner until, near 30 K, a broad shoulder-like drop appears. Below this shoulder, the resistivity decreases rapidly with temperature and at the lowest temperatures manifests T^2 behavior. The RRR value for this sample was 37 with $\rho_0 = 1.9\ \mu\Omega$ cm. As the applied pressure is increased, the shoulder shifts to lower temperatures and the resistivity data for temperatures just above the shoulder flattens.

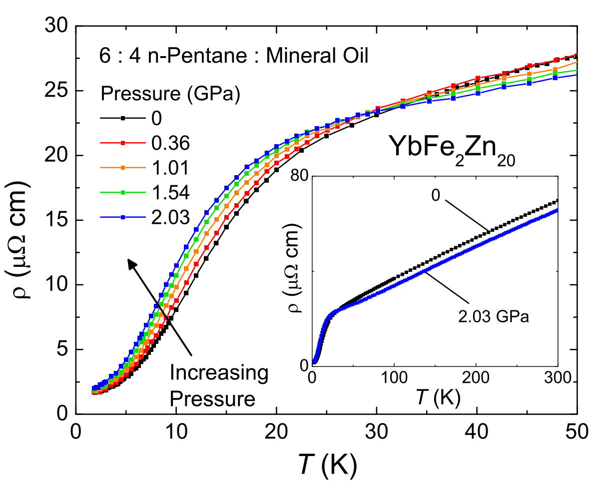

FIG. 1: (Color Online) Temperature dependent resistivity measurement of $YbFe_2Zn_{20}$ under pressure using a piston cylinder cell are shown up to 50 K for pressures up to 2.03 GPa. Inset: Full temperature range of the resistivity at ambient pressure and 2.03 GPa. The high temperature region shows typical metallic behavior with a near-linear dependence on temperature.

For measurements at higher pressures, the mBAC was used with both the 1 : 1 n-pentane : iso-pentane mixture and the 1 : 1 FC70 : FC770 mixture. Figure 2 shows resistivity measurements with an mBAC for pressures up to 5.14 GPa using 1 : 1 n-pentane : iso-pentane as the liquid pressure medium. At ambient pressure, the RRR value for this sample was 18 with $\rho_0 = 3.9\ \mu\Omega$ cm. As pressure is applied, a local maximum in the resistivity above the shoulder grows as the shoulder itself shifts to lower temperatures.

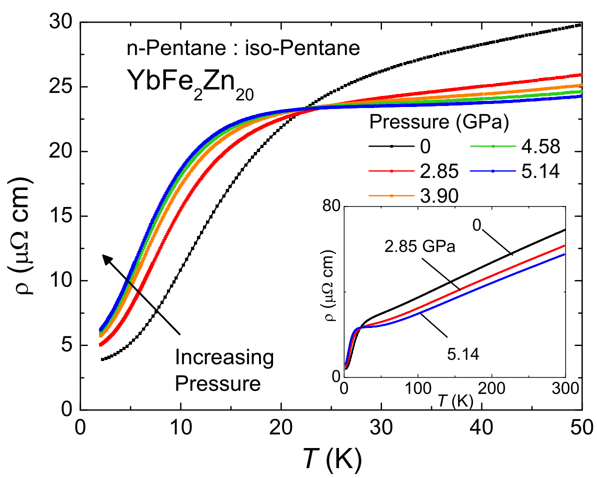

FIG. 2: (Color Online) Low temperature resistivity measurements under pressure using a modified Bridgman anvil cell with 1 : 1 n-pentane : iso-pentane as the liquid pressure medium, reaching a maximum pressure of 5.14 GPa. Inset: Resistivity curves for the full temperature range up to 300 K for pressures at 0, 2.85, and 5.14 GPa.

The $\rho(T) = \rho_0 + AT^2$ behavior that persisted up to about 11 K at ambient pressure is diminished to a lower temperature range and the upward curvature becomes steeper as pressure is increased. Measurements with the PPMS down to 2 K show quadratic behavior up to $\sim$ 3.3 K at 4.58 GPa (Fig. 3). $T_{\rm FL}$ was defined as the temperature at which the difference between experimental resistivity data, $\rho_{\rm exp}$, and linear fits to the $\rho_{\rm exp}$ versus T^2 data, $\rho_{\rm fit}$, became greater than 0.01 $\mu\Omega$ cm. For pressures where T^2 behavior was still observable above 2 K, $T_{\rm FL}$ was determined from measurements with the PPMS. For $T_{\rm FL}$ lower than 2 K, ^{3}He data were used for the quadratic fits.

In order to explore the possibility of magnetic ordering at lower temperatures, measurements of resistivity down to nearly 0.3 K for 4.20 and 4.73 GPa were taken using a ^{3}He cryostat, shown in Fig. 3. These measurements revealed no resistive anomalies down to almost 0.3 K and confirmed that T^2 behavior persists down to our lowest temperatures.

In order to achieve higher pressures, the 1 : 1 FC70 : FC770 liquid medium was used with the mBAC. Figure 4 shows selected resistivity curves for pressures up to 8.23 GPa from two different packings of the pressure cell (each using one half of the same crystal as a sample). At ambient pressure, the RRR values for the two samples used in these measurements are 26 and 25 with

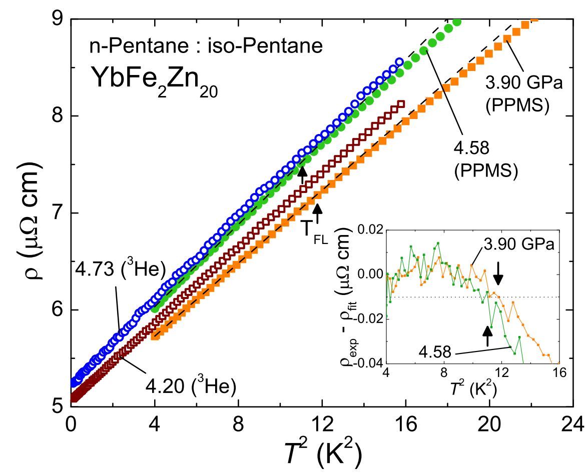

FIG. 3: (Color Online) T^2 dependence of resistivity at low temperatures for measurements with the PPMS at 3.90 and 4.58 GPa shown as the closed squares and circles, respectively, as well as measurements with the ^{3}He cryostat at 4.20 and 4.73 GPa denoted by the open squares and circles, respectively. The black dashed lines are linear fits to the low temperature data taken with the PPMS. The arrows indicate the temperature limit of T^2 behavior, $T_{\rm FL}$, from PPMS data. Inset: $\rho_{\rm exp} - \rho_{\rm fit}$ for both 3.90 and 4.58 GPa versus T^2. The black dotted line indicates a difference of -0.01 $\mu\Omega$ cm used to determine $T_{\rm FL}$.

$\rho_0 = 2.6$ and 2.8 $\mu\Omega$ cm, respectively. Under applied pressure, the resistivity in the high temperature region, between 30 and 300 K, continues to decrease with temperature (inset of Fig. 4) in a near-linear fashion. The broad shoulder once again changes into a broad maximum with pressure and further increases up to 8.23 GPa reveal this maximum sharpening.

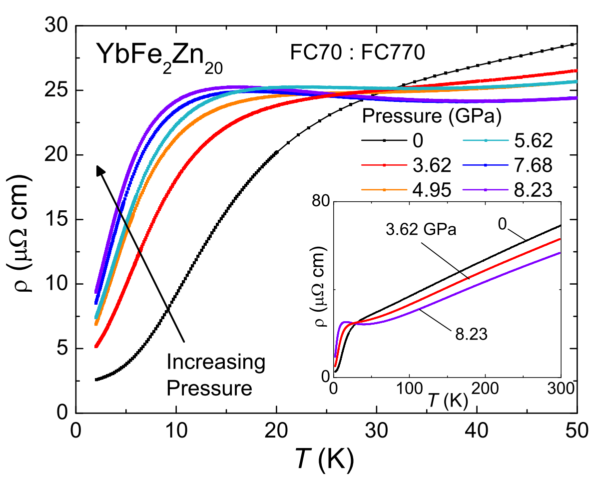

FIG. 4: (Color Online) Low temperature resistivity data for $YbFe_2Zn_{20}$ under pressures up to 8.23 GPa using 1 : 1 FC70 : FC770 as the liquid pressure transmitting medium. Selected curves are shown ($P = 0$, 3.62, 4.95, 5.62, 7.68, and 8.23 GPa) from two separate sets of measurements. Inset: Resistivity curves up to 300 K for $P = 0$, 3.62, and 8.23 GPa.

Measurements down to nearly 0.3 K were also conducted with 1 : 1 FC70 : FC770 as the liquid medium in the mBAC (Fig. 5). No features associated with magnetic ordering were seen in the data for pressures up to 8.23 GPa. Above 5 GPa, the range of T^2 behavior is suppressed to below 2 K. This decrease in $T_{\rm FL}$ continues with pressure and, at 8.23 GPa, the T^2 behavior is found only up to $T \sim 0.6$ K ($T^2 \sim 0.3$ K^2).

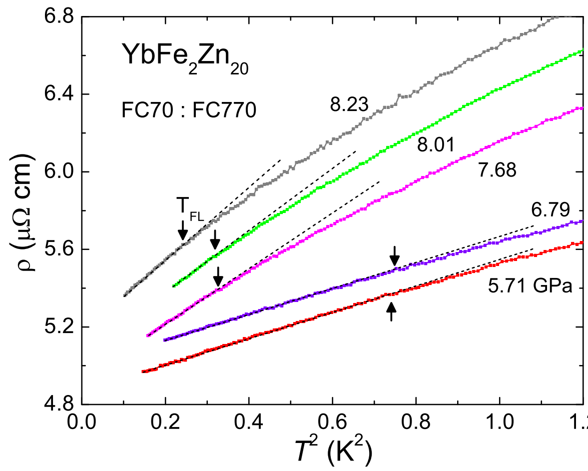

FIG. 5: (Color Online) T^2 dependence of resistivity at pressures of 5.71, 6.79, 7.68, 8.01, and 8.23 GPa from measurements with the ^{3}He cryostat. At maximum pressure, the T^2 region has greatly diminished. The black arrows indicate $T_{\rm FL}$ values that were determined as shown in the inset of Fig. 3.

IV. DISCUSSION

The application of pressure to Yb-based heavy fermion systems can shift the system from being dominated by the Kondo effect and manifesting low-temperature FL behavior, to being more local-moment like and even, in some cases, to manifesting long-range order.[30–33] In resistivity measurements of a Kondo lattice system, the logarithmic rise of resistivity due to the Kondo effect is countered by the coherent scattering of the electrons at lower temperatures, creating a local maximum in the resistivity. Since the Kondo temperature, $T_{\rm K}$, sets an energy scale for a crossover from a local moment to a Kondo-screened moment state and is not correlated with any sharp features in physical measurements, it becomes necessary to isolate the magnetic contribution from the resistivity data in order to help determine, or set limits on, $T_{\rm K}$. It is expected that the position of this local maximum scales with $T_{\rm K}$.[34–36]

The total resistivity of $YbFe_2Zn_{20}$ can be described as a combination of non-correlated, normal metal resistivity and a magnetic contribution to the resistivity. The normal metal resistivity, can be approximated by the temperature-dependent resistivity of $LuFe_2Zn_{20}$, which, with a full $4f$ shell, is a non-magnetic analogue to $YbFe_2Zn_{20}$. Both Yb and Lu curves are shown in the inset of Fig. 6. By taking the difference, $\rho_{mag} = (\rho - \rho_0)_{\rm Yb} - (\rho - \rho_0)_{\rm Lu}$, the partially filled $4f$ shell contribution to the resistivity can be effectively isolated. This is shown for several measurements under pressure in Fig. 6. For the subtraction, only the ambient pressure resistivity values of $LuFe_2Zn_{20}$ were used and is the likely cause of the negative ρ_{mag} values at higher temperatures.

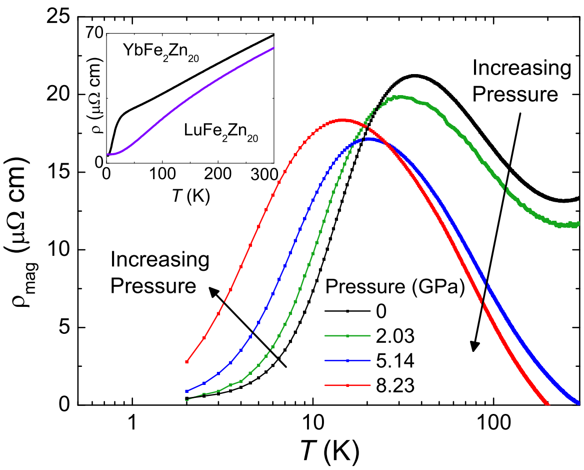

FIG. 6: (Color Online) The magnetic contribution, $\rho_{mag} = (\rho - \rho_0)_{\rm Yb} - (\rho - \rho_0)_{\rm Lu}$, to the total resistivity for various pressures are shown on a semi-log scale. The inset shows the ambient pressure curves for $YbFe_2Zn_{20}$ and its non-magnetic analogue $LuFe_2Zn_{20}$.

It is apparent that the low temperature maximum in the magnetic component of the resistivity decreases with pressure. For Kondo lattice systems, the electrons participating in the spin-dependent screening in the region of the Kondo temperature are intimately related to the Fermi-liquid quasiparticles at low temperatures. With previous results for $YbCo_2Zn_{20}$ having shown indications of a magnetic transition when $T_{\rm FL}$ was suppressed,[14–16] it is expected that a quantum critical point will also be reached when $T_{\rm FL}$ in $YbFe_2Zn_{20}$ has been driven to zero.

The suppressions of $T_{\rm max}$ and $T_{\rm FL}$ with pressure for $YbFe_2Zn_{20}$ are shown in Fig. 7. If the minimum of $T_{\rm max}$ is indeed an indicator that the system will manifest magnetic ordering,[15] then for $YbFe_2Zn_{20}$, the critical pressure may well be at a slightly higher pressure than the maximum achieved in this study. Furthermore, the Fermi-liquid state is almost completely suppressed by 8.23 GPa, another indicator that the system should be near its critical pressure value.

The influence of pressure on the Fermi-liquid behavior of $YbFe_2Zn_{20}$ is shown more clearly in Fig. 8. In Fig. 8(a), the spread of $T_{\rm FL}$ values seen at ambient pressure is small compared to the overall change in $T_{\rm FL}$ over the 8 GPa pressure range. At pressures near to but less than 5 GPa, measurements with the PPMS indicated quadratic temperature dependences still yet above

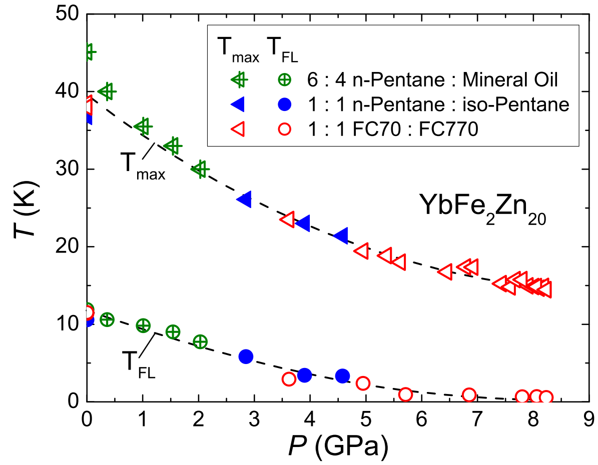

FIG. 7: (Color Online) $T_{\rm max}$ and $T_{\rm FL}$ as they evolve with pressure. The dashed lines are guides for the eye.

2 K. At these pressures, measurements extended down to ~ 0.3 K using a ^{3}He cryostat showed $T_{\rm FL}$ values close to those found using the PPMS (these are the two pairs of filled and half-filled symbols near 4 GPa in Fig. 8(a)). Although $T_{\rm FL}$ has not been driven to zero by our maximum pressure, extrapolation of $T_{\rm FL}(P)$ suggests that this will occur at higher pressures in the range of 9-10 GPa. The plot of the T^2 coefficient, A, as a function of pressure (Fig. 8(b)) shows divergent behavior with pressure, consistent with the diminishing $T_{\rm FL}$ and closeness to a quantum critical point.

The divergence of $A(P)$ is very clearly quantified in Fig. 8(c) where the progression of $A^{-1/2}$ with pressure is shown. A linear fit to the data, denoted by the black dashed line, shows that $A^{-1/2}$ will go to zero (indicating an infinitely large A value) at $\sim$ 9.8 GPa. These data indicate that $A \propto (P - P_{\rm c})^{-2}$ with $P_{\rm c} \simeq 9.8$ GPa. This simple and consistent functional dependence of A on pressure (even at higherst pressure and lowest T_{FL} values) suggests that the A values are not an artifact of the low temperature limitations of measurements in the ^{3}He temperature range.

It should be noted that data for $\rho_0(P)$ (not shown) does gradually increase from $P = 0$ to 8.23 GPa, effectively doubling in value from ambient to highest pressure.

At our highest pressures, A increases rapidly indicating a proximity to a quantum critical point near $P_{\rm c} = 9.8$ GPa. As pressure increases from atmospheric pressure to $\sim$ 8 GPa, we anticipate that the low temperature electronic specific heat, γ, increases. By using the Kadowaki-Woods plot in Fig. 4 of Ref. 7, we can predict an increase in γ from 520 mJ/mol K^2 to $\sim$ 2000 mJ/mol K^2 or greater at 8.23 GPa depending on whether all crystalline electric field split levels are comparable or lower than $T_{\rm K}$.

To further investigate the possibility that a QCP is being approached, an analysis of the progression of the power law behavior at low temperatures and high pres-

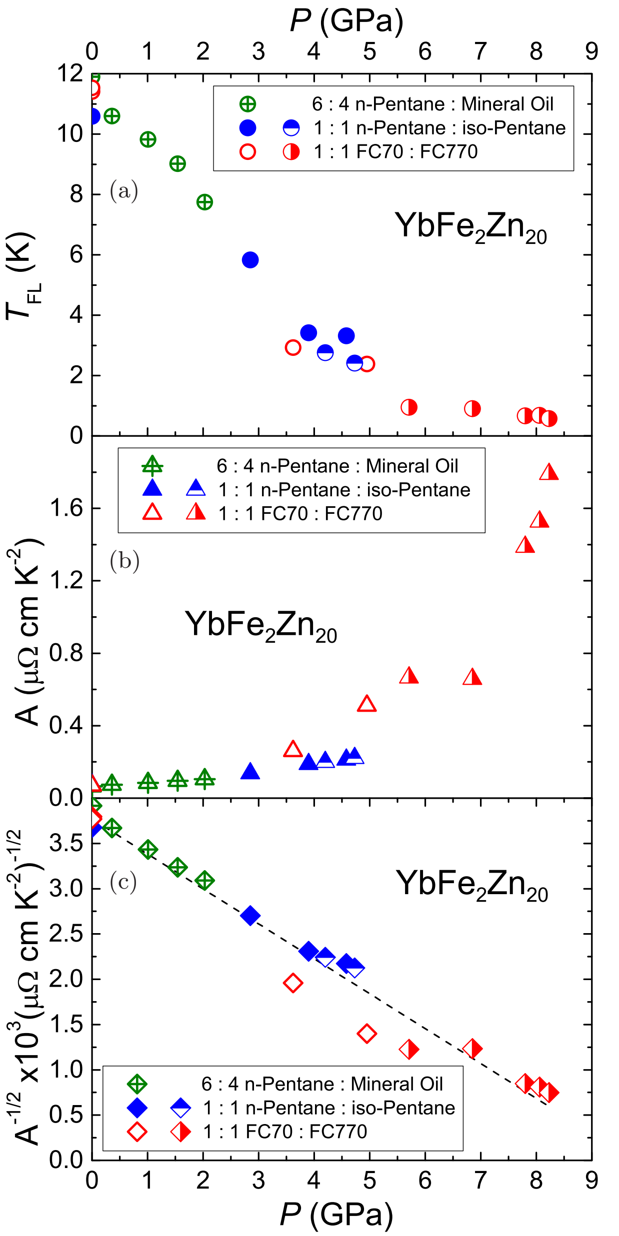

FIG. 8: (Color Online) (a) Evolution of $T_{\rm FL}$ as pressure is applied. By 8.23 GPa, $T_{\rm FL}$ is only as high as $\sim$ 0.6 K. Crossed, closed and open symbols are results from using the piston cylinder cell, the mBAC with the 1 : 1 n-pentane : iso-pentane mixture, and the mBAC with the 1 : 1 FC70 : FC770 mixture, respectively, in conjunction with the PPMS. Top half closed symbols and right half closed symbols indicate results from using the mBAC with the 1 : 1 n-pentane : iso-pentane mixture and the 1 : 1 FC70 : FC770 mixture, respectively, in conjunction with the ^{3}He cryostat. (b) T^2 coefficient ($\rho(T) = \rho_0 + AT^2$) which diverges as pressure is increased. (c) $A^{-1/2}$ as it progresses with pressure. The dashed line is a linear fit to the data with $A^{-1/2}$ reaching zero near 9.8 GPa.

sures was done. Figure 9 shows the results for pressures where measurements down to $\sim 0.3 - 0.4$ K were taken. Data from base temperature to 3 K are results from measurements in the ^{3}He cryostat and above 3 K, results from measurements in the PPMS. In this analysis, the lowest temperature ρ_0 from a T^2 fit was used for both sets of measurements.

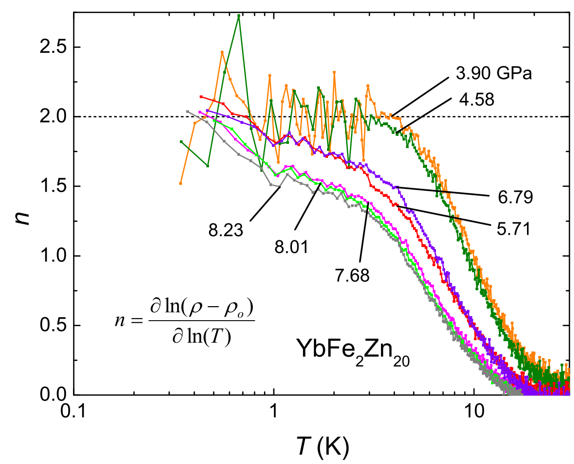

FIG. 9: (Color Online) Power law behavior for selected resistivity curves on a semilog scale. Data for $T < 3$ K are from measurements with a ^{3}He cryostat and data for $T > 3$ K are from measurements with the PPMS. The black dotted line is a guide for the eye and indicates a power of $n = 2$ for $\rho(T) = \rho_0 + AT^n$.

As expected, low pressure measurements show $n = 2$ at base temperatures across a decade of temperature. The large noise in the low temperature data for 3.90 and 4.58 GPa is restricted to one particular packing of the pressure cell (with higher noise) as the higher pressure n values (from different pressure cell packings) do not suffer from such large noise. For pressures above 4.58 GPa, $n = 2$ for a short range at low temperatures then gradually decreases as temperature increases. For the highest pressures where $P \geq 5.71$ GPa, $n = 2$ for only the lowest temperatures and instead shows n close to 1.5 for a significant temperature range. Since at our highest pressure, 8.23 GPa, is still below the expected $P_{\rm c} \approx 9.8$ GPa, it is still possible that by 9.8 GPa, the system will manifest an $n = 1.5$ power law behavior over a wider temperature range. If AFM order does arise at the critical pressure, this would be consistent with the results for spin fluctuation theories by Hertz and Millis as well as Moriya[37–39] where an $n = 1.5$ power law is predicted for a 3D AFM system. On the other hand, if ferromagnetic ordering occurs, $n \approx 1.33$ or 1.67 is predicted by Moriya[39] for 2D or 3D systems, respectively.

Another possibility is that instead of a QCP, we may be approaching a quantum critical region where neither Fermi-liquid behavior nor magnetic ordering exists and instead another exotic ground state may stabilize which is then followed by, at higher pressure, a magnetically ordered state.[40–45] It is evident that higher pressure measurements are necessary to further explore these possibilities.

V. CONCLUSION

The resistivity of $YbFe_2Zn_{20}$ was measured under pressure up to 8.23 GPa and down to temperatures of almost 0.3 K. Increasing pressure drives the characteristic Kondo temperature, T_K, to lower temperatures and diminishes the range of Fermi-liquid behavior. The dramatic enhancement of A as pressure increases to 8.23 GPa suggests a close proximity of $YbFe_2Zn_{20}$, at our highest pressure, to a quantum critical point where the system may develop a new magnetic ground state. Although not reached in this study, the critical pressure for $YbFe_2Zn_{20}$ can be inferred from $A(P) \propto (P - P_c)^{-2}$ to be $P_c \simeq 9.8$ GPa.

Acknowledgments

The authors would like to thank S. Jia and E. Mun for growing the $YbFe_2Zn_{20}$ samples used in this study and H. Hodovanets, and V. Taufour, for technical assistance and fruitful discussions. P.C.C. and S.L.B. would also like to thank J. Flouquet for useful comments about low temperature measurements. This work was carried out at Ames Laboratory, US DOE, under Contract # DE-AC02-07CH11358 (S.K.K., S.L.B. and P.C.C.). Part of this work was performed at the Iowa State University and supported by the AFOSR-MURI Grant # FA9550-09-1-0603 and also by the National Science Foundation under Grant # DMR-0805335 (M.S.T.). S.L.B. acknowledges partial support from the State of Iowa through Iowa State University.

[1] N. F. Mott, *Metal-Insulator Transitions: Second Edition* (Taylor & Francis, 1990).
[2] K. Bennemann and J. Ketterson, *Superconductivity: Novel superconductors* (Springer-Verlag Berlin Heidelberg, 2008).
[3] M. R. Norman, Science **332**, 196 (2011).
[4] G. R. Stewart, Rev. Mod. Phys. **56**, 755 (1984).
[5] G. R. Stewart, Rev. Mod. Phys. **73**, 797 (2001).
[6] G. R. Stewart, Rev. Mod. Phys. **78**, 743 (2006).
[7] M. S. Torikachvili, S. Jia, E. D. Mun, S. T. Hannahs, R. C. Black, W. K. Neils, D. Martien, S. L. Bud'ko, and P. C. Canfield, Proc. Natl. Acad. Sci. **104**, 9960 (2007).
[8] P. Canfield, S. Jia, E. Mun, S. Bud'ko, G. Samolyuk, and M. Torikachvili, Physica B **403**, 844 (2008).
[9] S. Jia, N. Ni, S. L. Bud'ko, and P. C. Canfield, Phys. Rev. B **80**, 104403 (2009).
[10] S. Jia, Ph.D. thesis, Iowa State University (2008).
[11] E. D. Mun, S. Jia, S. L. Bud'ko, and P. C. Canfield, Phys. Rev. B **86**, 115110 (2012).
[12] P. Coleman, in *Handbook of Magnetism and Advanced Magnetic Materials*, edited by H. Kronmuller and S. Parkin (John Wiley & Sons, Ltd, 2007), vol. 1, chap. 2, pp. 95–148.
[13] S. Doniach, Physica B+C **91**, 231 (1977).
[14] Y. Saiga, K. Matsubayashi, T. Fujiwara, M. Kosaka, S. Katano, M. Hedo, T. Matsumoto, and Y. Uwatoko, J. Phys. Soc. Jpn. **77**, 053710 (2008).
[15] K. Matsubayashi, Y. Saiga, T. Matsumoto, and Y. Uwatoko, J. Phys.: Conf. Ser. **200**, 012112 (2010).
[16] Y. Taga, S. Yoshiuchi, M. Ohya, J. Sakaguchi, Y. Hirose, F. Honda, T. Takeuchi, R. Settai, and Y. Ōnuki, Journal of the Physical Society of Japan **81SB**, SB064 (2012).
[17] S. Jia, S. L. Bud'ko, G. D. Samolyuk, and P. C. Canfield, Nat. Phys. **3**, 334 (2007).
[18] S. Jia, N. Ni, S. L. Bud'ko, and P. C. Canfield, Phys. Rev. B **76**, 184410 (2007).
[19] S. Jia, N. Ni, G. D. Samolyuk, A. Safa-Sefat, K. Dennis, H. Ko, G. J. Miller, S. L. Bud'ko, and P. C. Canfield, Phys. Rev. B **77**, 104408 (2008).
[20] P. C. Canfield and Z. Fisk, Philos. Mag. B **65**, 1117 (1992).
[21] P. C. Canfield, *Solution growth of intermetallic single crystals: a beginner's guide* (World Scientific, 2010), vol. 2 of *Book Series on Complex Metallic Alloys*, chap. 2, pp. 93–111.
[22] M. S. Torikachvili, S. L. Bud'ko, N. Ni, and P. C. Canfield, Phys. Rev. B **78**, 104527 (2008).
[23] M. S. Torikachvili, S. L. Bud'ko, N. Ni, P. C. Canfield, and S. T. Hannahs, Phys. Rev. B **80**, 014521 (2009).
[24] E. Colombier and D. Braithwaite, Rev. Sci. Instrum. **78**, 093903 (2007).
[25] A. Eiling and J. S. Schilling, J. Phys. F **11**, 623 (1981).
[26] G. J. Piermarini, S. Block, and J. Barnett, J. Appl. Phys. **44**, 5377 (1973).
[27] S. Klotz, J.-C. Chervin, P. Munsch, and G. L. Marchand, J. Phys. D **42**, 075413 (2009).
[28] T. Varga, A. P. Wilkinson, and R. J. Angel, Rev. Sci. Instrum. **74**, 4564 (2003).
[29] V. A. Sidorov and R. A. Sadykov, J. Phys.: Condens. Matter **17**, S3005 (2005).
[30] K. Alami-Yadri, H. Wilhelm, and D. Jaccard, Solid State Commun. **108**, 279 (1998).
[31] G. Knebel, D. Braithwaite, G. Lapertot, P. C. Canfield, and J. Flouquet, J. Phys.: Condens. Matter **13**, 10935 (2001).
[32] O. Trovarelli, J. Custers, P. Gegenwart, C. Geibel, P. Hinze, S. Mederle, G. Sparn, and F. Steglich, Physica B **312-313**, 401 (2002).
[33] H. Winkelmann, M. M. Abd-Elmeguid, H. Micklitz, J. P. Sanchez, C. Geibel, and F. Steglich, Phys. Rev. Lett. **81**, 4947 (1998).
[34] A. Yoshimori and H. Kasai, J. Magn. Magn. Mater. **31-34, Part 1**, 475 (1983).
[35] P. Coleman, J. Magn. Magn. Mater. **63-64**, 245 (1987).
[36] E. Bauer, R. Hauser, E. Gratz, K. Payer, G. Oomi, and T. Kagayama, Phys. Rev. B **48**, 15873 (1993).
[37] J. A. Hertz, Phys. Rev. B **14**, 1165 (1976).
[38] A. J. Millis, Phys. Rev. B **48**, 7183 (1993).
[39] T. Moriya and T. Takimoto, J. Phys. Soc. Jpn. **64**, 960

(1995).
[40] S. L. Bud'ko, E. Morosan, and P. C. Canfield, Phys. Rev. B **69**, 014415 (2004).
[41] S. L. Bud'ko, E. Morosan, and P. C. Canfield, Phys. Rev. B **71**, 054408 (2005).
[42] S. L. Bud'ko, V. Zapf, E. Morosan, and P. C. Canfield, Phys. Rev. B **72**, 172413 (2005).
[43] J. Custers, P. Gegenwart, C. Geibel, F. Steglich, P. Coleman, and S. Paschen, Phys. Rev. Lett. **104**, 186402 (2010).
[44] G. M. Schmiedeshoff, E. D. Mun, A. W. Lounsbury, S. J. Tracy, E. C. Palm, S. T. Hannahs, J.-H. Park, T. P. Murphy, S. L. Bud'ko, and P. C. Canfield, Phys. Rev. B **83**, 180408 (2011).
[45] E. D. Mun, S. L. Bud'ko, C. Martin, H. Kim, M. A. Tanatar, J.-H. Park, T. Murphy, G. M. Schmiedeshoff, N. Dilley, R. Prozorov, et al., Phys. Rev. B **87**, 075120 (2013).